

Synthesis and Evaluation of ^{18}F -Labeled Choline Analogs as Oncologic PET Tracers

Timothy R. DeGrado, Steven W. Baldwin, Shuyan Wang, Matthew D. Orr, Ray P. Liao, Henry S. Friedman, Robert Reiman, David T. Price, and R. Edward Coleman

Departments of Radiology, Chemistry, Surgery, Pediatrics, and Radiation Safety, Duke University Medical Center, Durham, North Carolina

Elevated levels of choline (trimethyl-2-hydroxyethylammonium) and choline kinase (CK) activity in neoplasms have motivated the development of positron-labeled choline analogs for noninvasive detection of cancer using PET. The aim of this study was to further evaluate [^{18}F]fluorocholine (fluoromethyl-dimethyl-2-hydroxyethylammonium [FCH]) as an oncologic probe in comparison with several other closely related molecules. **Methods:** FCH, [^{18}F]fluoromethyl-methylethyl-2-hydroxyethylammonium (FMEC), [^{18}F]fluoroethyl-dimethyl-2-hydroxyethylammonium (FEC), and [^{18}F]fluoropropyl-dimethyl-2-hydroxyethylammonium (FPC) were synthesized through [^{18}F]fluoroalkylation reactions. In vitro phosphorylation rates of the ^{18}F -labeled choline analogs and [*methyl*- ^{14}C]choline (CH) were studied using yeast CK. Several choline radiotracers were also evaluated in cultured PC-3 human prostate cancer cells. Data on chemical stability, radiation dosimetry, and toxicity of FCH were obtained. PET studies with FCH were performed on a patient with prostate cancer and a patient with a brain tumor. **Results:** FCH and FMEC revealed in vitro phosphorylation by CK that was similar to that of choline, whereas rates of phosphorylation of FEC and FPC were 30% ($P < 0.01$) and 60% ($P < 0.01$) lower, respectively. Accumulations of FCH, CH, and FPC in cultured PC-3 cancer cells were comparable, whereas uptake of FEC was approximately one fifth that of FCH. Dosimetry estimates using FCH biodistribution data in mice indicated that the kidneys are radiation-dose-critical organs for FCH. PET images of a patient with recurrent prostate cancer showed uptake of FCH in the prostatic bed and in metastases to lymph nodes. FCH PET showed uptake in malignancies in a patient with metastatic breast cancer. PET revealed FCH uptake in biopsy-proven recurrent brain tumor with little confounding uptake by normal brain tissues. **Conclusion:** The fluoromethyl choline analog FCH may serve as a probe of choline uptake and phosphorylation in cancer cells, whereas fluoroethyl (FEC) and fluoropropyl (FPC) analogs appear to have relatively poorer biologic compatibility. Preliminary PET studies on patients with prostate cancer and with breast cancer and brain tumor support further studies to evaluate the usefulness of FCH as an oncologic probe.

Key Words: choline; PET; prostate cancer; breast cancer; brain tumors

J Nucl Med 2001; 42:1805–1814

Use of PET imaging techniques for detection and localization of cancer in the body is based on the unique capability of PET to evaluate metabolic activity in human neoplasms. The glucose analog [^{18}F]FDG has proven useful as an oncologic PET probe for many forms of cancer on the basis of accelerated rates of glycolysis in malignancies (1–3). However, FDG PET has limited sensitivity for detection of certain cancer types, such as androgen-dependent prostate cancer, motivating efforts to develop new oncologic PET tracers.

^{11}C -Labeled choline (trimethyl-2-hydroxyethylammonium) (Fig. 1) (half-life = 20 min) has shown potential usefulness in 3 applications: brain tumors (4,5), for which FDG has suboptimal specificity because of uptake by normal brain and some posttherapy responses (6); prostate carcinoma (7), for which FDG has inadequate sensitivity (3,8); and esophageal carcinoma (9), for which background activity with FDG limits detection of neoplasms in the mediastinum. The practical advantages of working with the longer-lived radioisotope ^{18}F (half-life = 110 min) led Hara et al. (10) to synthesize and preliminarily evaluate the choline analog 2-[^{18}F]fluoroethyl-dimethyl-2-hydroxyethylammonium (FEC) (Fig. 1). We recently reported the synthesis and preliminary evaluation of no-carrier-added [^{18}F]fluorocholine (fluoromethyl-dimethyl-2-hydroxyethylammonium [FCH]) as a PET probe of prostate cancer (11) (Fig. 1). On the basis of structural similarity, we anticipated that the [^{18}F]fluoromethylated FCH would mimic choline transport and metabolism more closely than that of the [^{18}F]fluoroethylated FEC, resulting in physiologic processing closer to that of choline. In this study, the uptakes of FCH, FEC, and other structurally similar choline analog tracers were evaluated for their biologic acceptance for phosphorylation by choline kinase (CK) and uptake by cultured PC-3 human prostate cancer cells. Preliminary data on chemical stability, toxicity, and radiation dosimetry for FCH are reported. Finally, FCH PET was performed on a patient with prostate cancer and a patient with a brain tumor.

MATERIALS AND METHODS

Synthesis of Radiotracers

[*methyl*- ^{14}C]Choline (CH) was obtained from NEN Research Products (Boston, MA). No-carrier-added FCH was synthesized by reacting [^{18}F]fluorobromomethane ([FBM] isolated by gas

Received Sep. 22, 2000; revision accepted Feb. 14, 2001.

For correspondence or reprints contact: Timothy R. DeGrado, PhD, Department of Radiology, Duke University Medical Center, Box 3949, Durham, NC 27710.

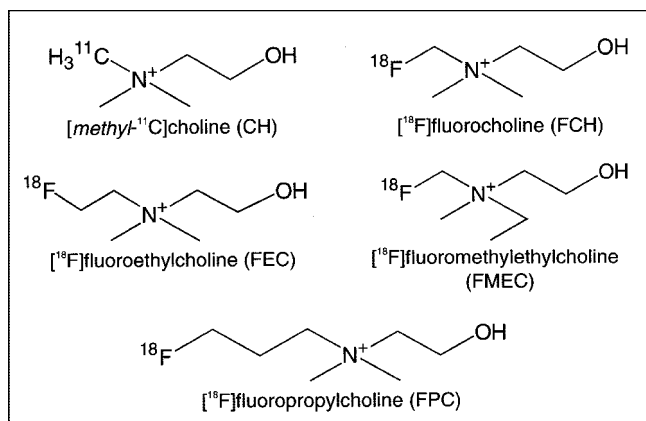


FIGURE 1. Chemical structures of positron-labeled choline analogs.

chromatography [GC] with dimethylethanolamine as modified from DeGrado et al. (11). In an analogous fashion to the synthesis of FCH, [¹⁸F]FEC was synthesized through the intermediate 1-[¹⁸F]fluoro-2-bromoethane (FBE) by radiofluorination of 1,2-dibromoethane rather than dibromomethane. For isolation of FBE, the temperature of the preparative GC column (Porapak Q, 80–100 mesh, 7.8 × 700 mm; Alltech Associates Inc., Deerfield, IL) was maintained at 135°C. [¹⁸F]Fluoromethyl-methylethyl-2-hydroxyethylammonium (fluoromethylethylcholine [FMEC]) (Fig. 1) was synthesized by reaction of FBM with ethylmethylethanolamine (Pfaltz and Bauer, Waterbury CT) by the same procedure as for synthesis of FCH. [¹⁸F]Fluoropropyl-dimethyl-2-hydroxyethylammonium (fluoropropylcholine [FPC]) (Fig. 1) was produced through the intermediate [¹⁸F]fluorobromopropane (FBP), which was synthesized and purified by high-performance liquid chromatography (HPLC) as described (12). The syntheses of FBE and FBP were not optimized, resulting in poorer radiochemical yields of FEC (<3%) and FPC (<1%), respectively, than for FCH or FMEC (30%–40%).

The radiochemical purity of the ¹⁸F-labeled choline analogs was monitored by cation-exchange HPLC as described for measurement of CH metabolites (13). The column was Partisil SCX (250 × 4.6 mm; Alltech Associates) eluted by 0.25 mol/L sodium dihydrogen phosphate solution (pH 4.8) and acetonitrile (90:10) at a flow rate of 1.8 mL/min. Radioactivity and ultraviolet absorbance (206 nm) of the eluent were measured in series. The retention times were 5.0, 5.4, 5.5, and 6.0 min for FCH, FEC, FMEC, and FPC, respectively (Fig. 2). The cation-exchange HPLC system was found to be preferable to the reverse-phase HPLC system originally developed for quality assurance of FCH (11) because peak resolution was superior, and retention of radioactivity on the column was negligible.

Two modifications were implemented to the FCH synthesis procedure since its original publication (11). To ensure removal of trace quantities of dimethylethanolamine from the product, the transfer of material from the fluoroalkylation reaction vessel to the cation-exchange Sep-Pak cartridge (ACCEL Light CM; Waters, Milford, MA) was performed using ethanol instead of water, and the Sep-Pak cartridge was washed with an additional 5 mL ethanol. The subsequent washing of the cartridge with 10 mL water and elution of FCH from the cartridge with isotonic saline were performed as described (11). The second modification was the introduction of a cleansing procedure for the GC column used to purify

FBM or FBE. After each run, 20 mL ethanol were back flushed through the GC column followed by 2 h of back purging of the column with helium. This procedure ensures that remains of dibromomethane and its decomposition products do not build up on the GC column and eventually contaminate the FBM or FBE product.

Stability of FCH

The stability of FCH in its prepared form was evaluated by monitoring the radiochemical purity using the HPLC system described above. Furthermore, the stability of FCH in blood was examined by incubating approximately 3.7 MBq FCH in a 3-mL sample of heparinized whole blood taken from healthy human

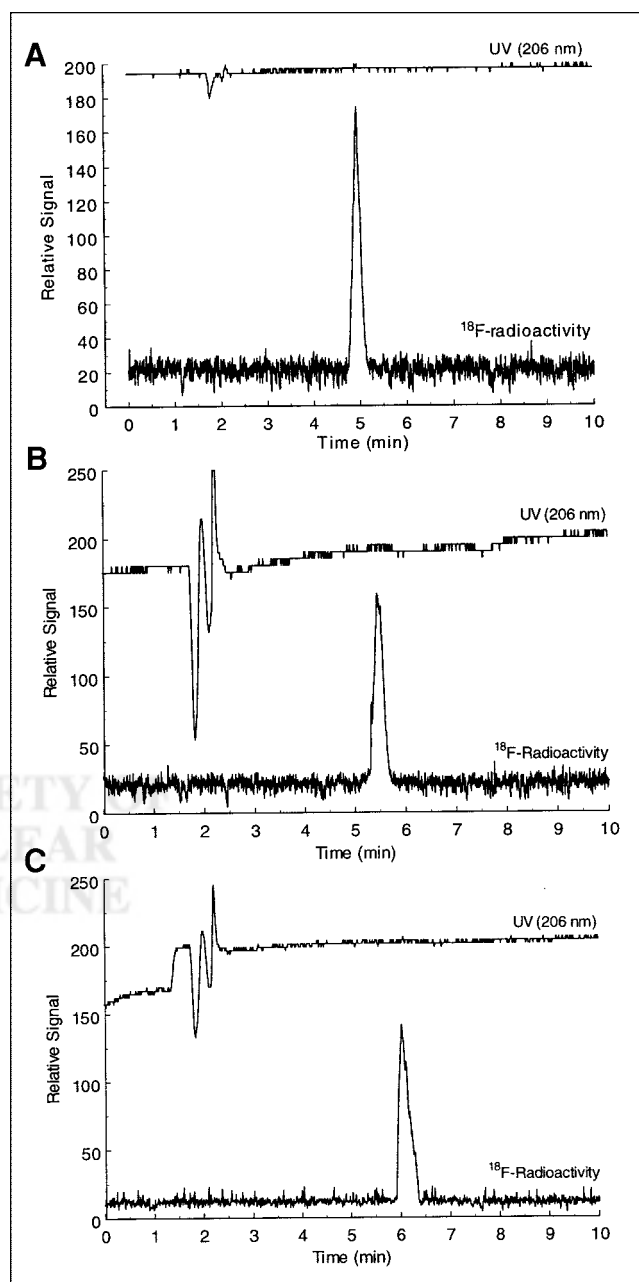


FIGURE 2. Cation-exchange HPLC radiochromatograms of FCH (A), FEC (B), and FPC (C) final products. UV = ultraviolet.

subjects ($n = 5$). After a 2-h incubation at 37°C, the plasma was separated, the plasma proteins were precipitated by adding 2 volumes of methanol, and the supernatant was analyzed for intact FCH by cation-exchange HPLC.

Analysis of Hydrophilic Choline or FCH Metabolites in Biologic Samples

The primary hydrophilic metabolites of choline in mammals are phosphocholine and betaine. If FCH is handled similarly biochemically to CH in cancer cells, then ^{18}F -labeled phosphorylfluorocholine (P-FCH) and fluorobetaine (FB) may be formed. To measure the levels of FCH, FB, and P-FCH in biologic samples, a modification of the gradient-HPLC method of Pomfret et al. (14) was used. ^{14}C -Labeled betaine and phosphocholine were prepared enzymatically from commercially available CH (NEN Research Products) using choline oxidase (13) and CK (15), respectively. The HPLC system used a microprocessor-controlled solvent delivery system and a silica column (Adsorbosphere silica [10 μm], 250 \times 4.6 mm; Alltech Associates). The column was kept at room temperature and the flow rate was maintained at 1.5 mL/min. Buffer A contained acetonitrile, ethanol, acetic acid, 1.0 mol/L ammonium acetate, water, and 0.1 mol/L sodium phosphate (800:68:2:3:127:10 [v/v]) and buffer B contained the same constituents but in different proportions (400:68:44:88:400:10 [v/v]). Fractions of effluent were collected every 0.5 min and counted first for ^{18}F radioactivity in a well counter for experiments involving FCH and then transferred to scintillation vials for counting ^{14}C radioactivity. The column was equilibrated for 6 min with buffer A before injection. After the injection (<100 μL), buffer A was delivered for 6 min, which eluted betaine (3 min) from the column. Over a period of 10 min, solvents were switched to 100% buffer B using a linear gradient, during which time FCH (12.5 min) and choline (15 min) were eluted. Buffer B was then delivered for a further 9 min, eluting phosphocholine (19.5 min). Reequilibration of the column with 100% buffer A for 6 min preceded the next injection.

In Vitro Phosphorylation of FCH by Yeast CK

To determine whether FCH is a substrate for CK, FCH (0.9–1.8 MBq) and CH (74–150 kBq) were incubated in a test tube with yeast CK (25 milliuunits [mU]/mL), choline (1–10,000 $\mu\text{mol/L}$), MgCl_2 (12.5 mmol/L), and ATP (10 mmol/L) in Tris \cdot HCl buffer (0.1 mol/L, pH 8.75) for 10 min at 23°C. The test tube was gently agitated throughout the incubation period. Tubes were placed in a boiling water bath for 2 min to stop the reaction. To serve as controls, some samples were placed directly in the boiling water bath after addition of all substrates. The phosphorylated fraction of each radiotracer was isolated from the nonmetabolized fraction by anion-exchange chromatography according to the method of Ishidate and Nakazawa (15) and counted in a well counter or a scintillation counter. The percentage of radioactivity converted to the phosphorylated form was calculated. Preliminary studies showed the phosphorylated fraction to rise linearly with time for incubations of <15 min.

Uptake and Metabolism of Radiotracers by PC-3 Human Prostate Cancer Cells

Cells (2.5×10^5 per well) were seeded on 6-well plates and incubated for 2 d, at which time >90% confluence was reached. The incubation medium was Dulbecco's modified Eagle's medium (DMEM) supplemented with 10% calf serum. The medium contained 15 mmol/L glucose. On the day of the study, the medium was refreshed using a volume of 1 mL in each well. Cells were

incubated under control conditions or with the addition of metabolic and growth factor receptor inhibitors to test the sensitivity of uptake of the radiotracers to specific inhibition. The inhibitor of choline uptake and phosphorylation, hemicholinium-3 (HC-3) (Research Biochemicals, Natick, MA), was added to give a concentration of 5 mmol/L. The concentration of the inhibitor was approximately 10 times the literature *in vivo* inhibitory concentration of 50% (IC_{50}) for choline phosphorylation (16). After a 30-min incubation period, the radiotracers were added (~74 kBq per well) in separate wells and the cells were incubated at 37°C for 2 h. The radioactive medium was removed and the cells were washed 3 times with phosphate-buffered saline solution, released from the plates by incubating briefly with 0.05% trypsin in DMEM, transferred to test tubes, and counted for radioactivity in a γ -counter (^{18}F) or a liquid scintillation counter (^{14}C). The amount of radioactivity in the cells was normalized by the dose administered to each well.

Preliminary analysis of radiolabeled metabolites of FCH and CH in PC-3 cells was performed. Cells were incubated in 6-well plates with a mixture of FCH (~3.7 MBq) and [^{14}C]CH (~74 kBq) for 2 h as described above, followed by removal of radioactive medium and 3 rinses with phosphate-buffered saline solution. Methanol (1 mL) was added to each well and the cells were lysed by maintaining the temperature at 37°C for 30 min. The methanol phase was transferred to a glass test tube. Each well was rinsed with an additional 0.5 mL methanol that was added to the original fraction. To each tube, 3 mL chloroform and 1 mL 0.25 mol/L sodium phosphate (pH 4.5) were added to separate lipids from water-soluble molecules. After vigorous mixing of the samples for 1 min, the 2 phases were separated, and a 0.5-mL aliquot of each phase was counted for ^{18}F and ^{14}C radioactivity. The aqueous phase was further analyzed for water-soluble metabolites using the gradient-HPLC method described earlier. Radioactivity in the metabolite fractions (lipid, CH/FCH, [^{14}C]-betaine/FB, [^{14}C]-phosphocholine/P-FCH) was expressed as the percentage of total radioactivity administered to each well.

Human Dosimetry Estimation

Tissue distribution data (percentage dose per gram of tissue) obtained in a mouse model after injection of FCH (11) were converted to the percentage dose per organ using the method of Kirschner et al. (17). The distribution was assumed to be static at >10 min after injection, consistent with the long retention of the tracer in tissue (11). These data were entered into the MIRDose 3.1 program (18) to calculate dose estimates. Urinary radioactivity was assumed to be retained within the urinary bladder. Thus, assumptions made in these calculations would tend to overestimate the radiation dose in human imaging studies in which urinary radioactivity may be voided after the imaging study is performed. Because urinary excretion patterns in rodents are commonly more rapid than those in humans, the assumption of no urinary clearance of radioactivity was precautionary. Bone uptake was distributed at the bone surfaces. The look-up table corresponding to a 70-kg adult male Oak Ridge National Laboratory phantom was used because this would best reflect the primary study population (prostate carcinoma).

Toxicity Study

Four unanesthetized BALB/c nude mice were administered 1 mg/kg [^{19}F]FCH through tail vein injection and monitored for 48 h. This dose represented an approximately 300,000-fold excess of

FCH in comparison with the normal dose that a 70-kg person would receive in a FCH PET study. The mice were killed at 48 h.

PET Studies

The biodistribution of FCH was investigated in a patient with prostate cancer, a patient with metastatic breast cancer, and a patient with a brain tumor. The FCH PET studies were approved by the Duke University Medical Center Institutional Review Board and Cancer Research Committee. The subjects were informed of all risks associated with the study and written informed consent was obtained. Patient 1 had undergone prostatectomy and radiation therapy and was being evaluated for recurrence of prostate cancer. Patient 2, having previously undergone resection of an astrocytoma, was also being evaluated for recurrence of disease. Patient 3 was a 50-y-old breast cancer patient who had undergone mastectomy 3 y earlier, followed by tamoxifen chemotherapy. Imaging was performed using an Advance PET scanner (General Electric Medical Systems, Milwaukee, WI) with an intrinsic spatial resolution of ~5 mm in all directions (19). A transmission scan of the pelvic region was obtained before administration of radiotracer. [¹⁸F]FCH (93–185 MBq) was administered intravenously. In the first patient dynamic imaging of the lower pelvic region commenced for 10 min (frame sequence = 12 × 10 s, 8 × 1 min). After the dynamic scan, a whole-body emission scan (4 min per bed position) was obtained without attenuation correction. In the patient with a brain tumor, a 4-min transmission scan of the head preceded the injection of radiotracer. For the breast cancer and brain tumor patients, FDG PET images were acquired within 1 wk of the FCH PET scan. Approximately 370 MBq FDG were administered intravenously, and emission imaging commenced at 45 min after injection. The emission imaging of the brain was performed in 3-dimensional scanning mode (septa out), whereas imaging of the body was performed in 2-dimensional mode (septa in). The images were reconstructed using an ordered subset expectation maximization algorithm. Regions of interest (ROIs) were drawn manually on the attenuation-corrected images for evaluation of FCH kinetics in tissues. Standardized uptake values (SUVs) of FCH uptake in tissues were calculated using the attenuation-corrected images according to the equation:

$$\text{SUV} = \frac{\text{Body Weight (g)} C_{\text{FCH}} (\text{Bq/mL})}{\text{Dose (Bq)}}$$

where C_{FCH} is the concentration of FCH in the tumor ROI. In the breast cancer patient, SUVs for FDG uptake within tumors were calculated similarly using similar ROIs drawn on the FDG scans.

Statistical Methods

Results are expressed as mean ± SD. Statistical analysis was performed using the Student *t* test, and statistical significance was inferred at $P < 0.05$.

RESULTS

Stability of FCH

The radiochemical purity of the FCH preparation was >99% as monitored by cation-exchange HPLC. Radioactivity concentration was 37–185 MBq/mL. The radiochemical purity remained >99% after maintenance of the FCH preparation at room temperature for 7 h. FCH was also found to be stable in blood samples taken from healthy human subjects ($n = 5$). HPLC analysis showed FCH to be

completely intact after 2-h incubations in whole-blood samples at 37°C.

In Vitro Phosphorylation of FCH by Yeast CK

To determine whether FCH is a substrate for CK, FCH and [¹⁴C]choline (CH) were incubated with yeast CK (25 mU/mL) and choline (1–10,000 μmol/L) for 10 min at 23°C. Samples quenched by boiling before incubation showed negligible phosphorylation activity. Figure 3 shows that, after separation from unreacted FCH and CH using an anion-exchange resin (15), a single, more polar chemical product is formed from FCH and CH. The ¹⁴C-labeled product exhibited the same retention time as an authentic standard for unlabeled phosphocholine, seen by in-series ultraviolet detection. The presence of a single ¹⁸F-labeled product and the similar relationship of retention times between FCH and CH (Fig. 3A) and their phosphorylated products (Fig. 3B) suggest that the ¹⁸F-labeled product is P-FCH. Figure 4 shows the dependence of phosphorylation rate on choline concentration, displaying a similar sigmoid relationship for both radiotracers that is typical of Michaelis-Menten kinetics.

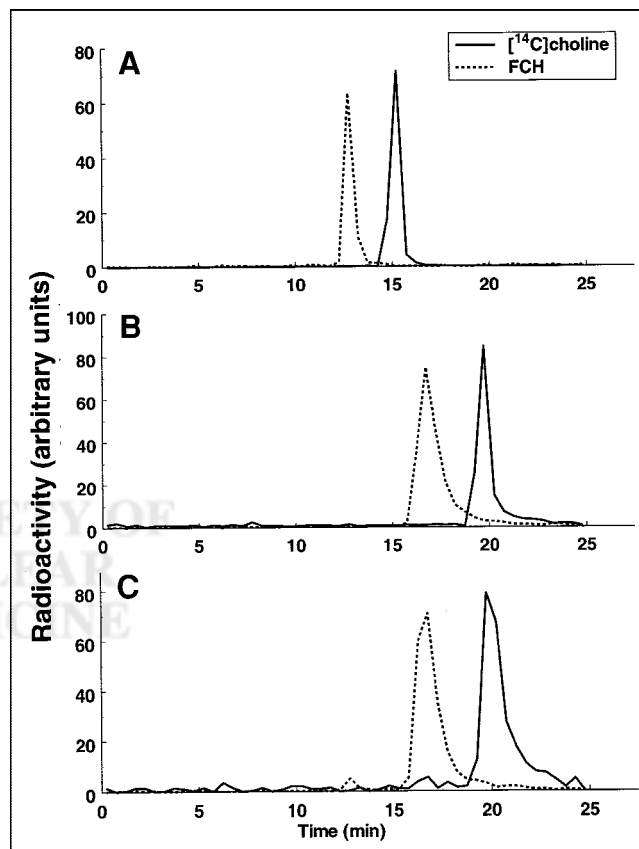


FIGURE 3. Normal phase, gradient-HPLC analysis of FCH and [¹⁴C]CH (A); P-FCH and [¹⁴C]phosphoryl-CH enzymatically synthesized using yeast CK according to method of Ishidate and Nakazawa (15) (B); and hydrophilic radiolabeled metabolites in cultured PC-3 prostate cancer cells after incubation with FCH and CH (C). Close correspondence of chromatograms B and C indicates extensive intracellular phosphorylation of FCH and CH in cancer cells.

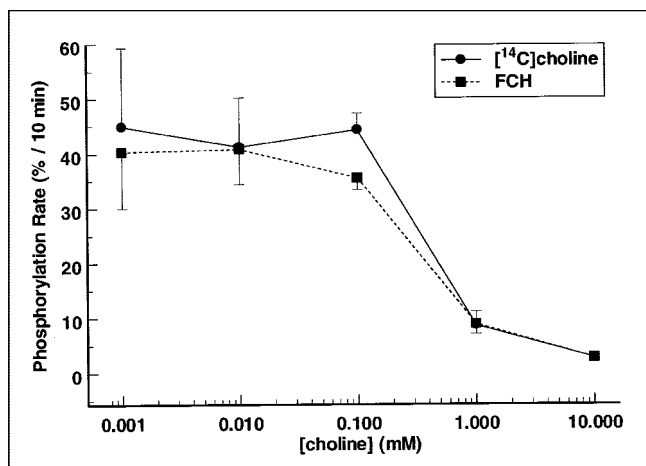


FIGURE 4. In vitro phosphorylation of FCH and CH by CK. Incubations were performed at room temperature with 25 mU/mL CK over choline concentrations of 0.001–10 mmol/L. Each data point represents results as mean \pm SD of 3 samples. Similar inhibition of FCH and CH phosphorylation at higher choline concentrations is indicative of competitive inhibition of FCH phosphorylation by choline.

lis–Menten-type kinetics. The apparent IC_{50} values for inhibition of phosphorylation of radiotracer by choline were ~ 0.4 mmol/L for FCH and CH. The phosphorylation rates were similar for FCH and CH at all choline concentrations. At a low choline concentration of 1 μ mol/L, phosphorylation rates of FCH and FMEC were equivalent to that of CH, whereas phosphorylation rates of FEC and FPC were approximately 30% and 60% less than that of FCH, respectively (Table 1).

Accumulation of Choline Analogs by Cultured PC-3 Prostate Cancer Cells

Under control conditions, cultured PC-3 human prostate cells accumulated FCH similar to that of CH (Table 1). However, the fluoroethylated analog, FEC, showed only one fifth of the uptake of FCH ($P < 0.01$). The fluoromethylethyl analog, FMEC, showed an accumulation higher than that of FEC ($P < 0.05$) but lower than that of FCH ($P < 0.01$). Uptake of the fluoropropyl analog, FPC, was not significantly different from that of FCH. Specific inhibition of choline transport and phosphorylation by HC-3 resulted in 89% ($P < 0.001$), 45% ($P < 0.01$), and 41% decreases in uptakes of FCH, CH, and FPC, respectively.

Analysis of Metabolites of FCH and [¹⁴C]CH in Cultured PC-3 Prostate Cancer Cells

A preliminary analysis of the chemical form of radioactivity present in PC-3 cells incubated with FCH and CH was performed. Cells incubated in 6-well plates for 2 h with radiotracers were washed thoroughly to remove all extracellular radioactivity. The cells were lysed in methanol, and the methanol solution was added to chloroform to solubilize all lipophilic metabolites. The hydrophilic metabolites were extracted with 0.25 mol/L sodium phosphate solution (pH

4.8) and subjected to gradient-HPLC analysis for measurement of radioactivity in the form of FCH/CH, FB/betaine, and P-FCH/phosphocholine. Table 2 shows the results expressed as percentage of administered dose to each well. CH and FCH were found to undergo extensive metabolism within the PC-3 cells. Approximately 72% of ¹⁸F radioactivity was indicated to be P-FCH, whereas 91% of ¹⁴C radioactivity was found as [¹⁴C]phosphocholine (Table 2; Fig. 3). Radiolabeled lipophilic metabolites of FCH comprised 25% of the total ¹⁸F radioactivity, whereas lipophilic metabolites of CH represented only 7% of the total ¹⁴C radioactivity. A 5-fold higher incorporation of radioactivity into lipophilic species for FCH was found relative to CH. Neither [¹⁴C]betaine nor its ¹⁸F-labeled counterpart was detected by HPLC analysis, indicating that oxidation of FCH and CH in the cancer cells was negligible.

Human Dosimetry Estimates

Table 3 gives the radiation dose estimates to human organs as determined from calculations based on mouse FCH biodistribution data (11). To produce conservative estimates, the total-body residence time was assumed to be determined solely from radioactive decay ($1.44 \times$ half-life = 2.6 h). The effective dose equivalent from a 370-MBq administration was estimated to be 0.01 Sv, which is below the Food and Drug Administration (FDA) single-study limit of 0.03 Sv for research subjects. However, the largest organ radiation dose (kidney) was 0.081 Gy/370 MBq injected, which is above the 0.05-Sv single-organ dose per study established by the FDA for research studies. Therefore, it was determined that the maximum administered dose in the initial studies with FCH would be 220 MBq. Refinement of these dosimetry estimates is needed using biodistribution data in humans in a subsequent study with larger numbers of subjects.

Toxicity Study

Acute toxicity of [¹⁹F]FCH (1 mg/kg of body weight) was determined in 4 untreated BALB/c mice. No deaths were

TABLE 1
In Vitro Phosphorylation Rate and Cellular Uptake of Radiolabeled Choline Analogs

Tracer	In vitro phosphorylation* (%)	Uptake by PC-3 cancer cells (% dose/2 h/10 ⁵ cells plated)	
		Control	HC-3 (5 mmol/L)
CH	55.9 \pm 11.0	1.88 \pm 0.25	1.04 \pm 0.11
FCH	62.0 \pm 8.8	1.58 \pm 0.18	0.18 \pm 0.02
FMEC	55.2 \pm 6.6	0.74 \pm 0.04 [†]	0.12 \pm 0.02
FEC	43.4 \pm 3.4 [†]	0.32 \pm 0.05 [†]	NA
FPC	22.1 \pm 3.1 [†]	1.29 \pm 0.28	0.76 \pm 0.20

*Tracers incubated in 1 μ mol/L choline and 25 mU/mL yeast CK at 23°C for 10 min ($n = 5$ samples each).

[†] $P < 0.01$ vs. FCH.

NA = not available.

TABLE 2

Analysis of Radioactive Intracellular Metabolites of CH and FCH in Cultured PC-3 Cancer Cells

Condition	¹⁴ C-Labeled species			¹⁸ F-Labeled species		
	Lipophilic metabolites	Hydrophilic metabolites		Lipophilic metabolites	Hydrophilic metabolites	
		CH	Phosphocholine		FCH	P-FCH
Control	0.44 ± 0.19	0.16 ± 0.06	5.9 ± 2.3	2.4 ± 0.4*	0.29 ± 0.05	7.1 ± 0.9
+HC-3†	0.06 ± 0.03	0.14 ± 0.13	0.08 ± 0.08‡	0.01 ± 0.01‡	0.04 ± 0.01‡	0.12 ± 0.03‡

*P < 0.01 vs. ¹⁴C, same metabolite fraction and condition.

†Uptake and phosphorylation of CH and FCH inhibited with 5 mmol/L HC-3.

‡P < 0.01 vs. control condition, same radiolabel and metabolite fraction.

Tracers were incubated for 2 h in approximately 5 × 10⁵ cells at 37°C (n = 3 samples each). Values are expressed as percentage of administered dose of radioactivity after removal of radioactive medium and 3 rinses with phosphate-buffered saline.

observed in the mice up to 48 h after administration of [¹⁹F]FCH. Nor were any behavioral or movement abnormalities observed by casual inspection during the monitoring period. On the basis of our estimates of specific activity of the FCH (~74 GBq/μmol), the normal dose of FCH in the radiotracer preparation would be a factor of ~300,000 times lower than the dose given in this toxicity study.

PET in Patients

Patient 1. A 66-y-old man was initially diagnosed 5 y earlier with locally advanced clinical stage T3 N0 M0 prostate cancer and underwent radical prostatectomy followed by external beam radiation to the prostate bed. His serum prostate-specific antigen (PSA) was 2.0 ng/mL after therapy. The patient then underwent androgen-deprivation therapy. Because his serum PSA began rising at approximately 1 y before PET scanning, the chemotherapy was discontinued. The current serum PSA of the patient was 40.1 ng/mL. Recent radionuclide bone scans showed no abnormalities, whereas CT of the chest, abdomen, and pelvis showed only small lymph nodes (~1 cm) in the pelvis and mediastinum. FCH PET images acquired at 2–4 min revealed accumulation of FCH in the prostate bed before the arrival of activity at the bladder (Fig. 5A). Figure 5B shows the kinetics of FCH in the prostate bed and ROIs drawn

within the urinary bladder and iliac artery. The arterial concentration of FCH peaked early and fell rapidly to <5% of the peak level within 2 min after injection, indicating extremely rapid blood clearance. Radioactivity concentration rose rapidly in the prostate bed and reached a plateau by 3 min after injection. Radioactivity began to arrive in the bladder at 4–5 min after injection and the concentration increased rapidly thereafter. The whole-body images showed abnormally high foci of FCH uptake in the chest suggestive of prostate cancer within mediastinal lymph nodes (Fig. 5C).

Patient 2. A 23-y-old woman was evaluated by FCH PET and FDG PET for recurrence of a previously resected anaplastic astrocytoma (Fig. 6). The PET images were coregistered with T1-weighted magnetic resonance (MR) images using Gd-diethylenetriaminepentaacetic acid contrast enhancement. The FCH PET images showed marked uptake in regions of the wall of the surgical cavity. The low concentration of tracer in the normal cerebral cortex allowed excellent delineation of the tumor from normal brain. The maximal tumor-to-cortex ratio was ~10:1 and was attained within 5 min after injection. Most, but not all, of the FCH-avid regions corresponded with Gd-enhanced regions on the MR images. Biopsies taken from the cavity wall confirmed recurrence of the tumor. The FDG PET images indicated a thin rim of increased FDG uptake located posteriorly on the cyst wall, but the boundary of the tumor could not be reliably determined because of high uptake of FDG by normal cortex.

Patient 3. A 50-y-old woman had undergone reexcision of right breast intraductal carcinoma 4 y earlier and then right modified radical mastectomy 3 y earlier followed by tamoxifen chemotherapy. Six months before the PET scans, metastatic breast cancer was detected by palpation (right breast sternal mass) and CT (mediastinal and hilar adenopathies, mass in right anterior pelvis). Tamoxifen therapy was stopped. The FDG PET scan showed uptake of tracer in the sternal mass (SUV, 5.0), mediastinal and hilar adenopathies (SUVs, ~5.5), and the pelvic tumor (SUV, 9.5) (Fig. 7). Uptake of FCH was also observed in the corresponding

TABLE 3

Human Radiation Dose Estimates for FCH

Tissue	Dose (mSv/MBq)
Heart	0.0124
Brain	0.0019
Lung	0.0116
Liver	0.081
Kidney	0.219
Bone	0.0103
Muscle	0.0086
Red marrow	0.0116
Testes	0.0076
Ovaries	0.0105
Bladder wall	0.0132

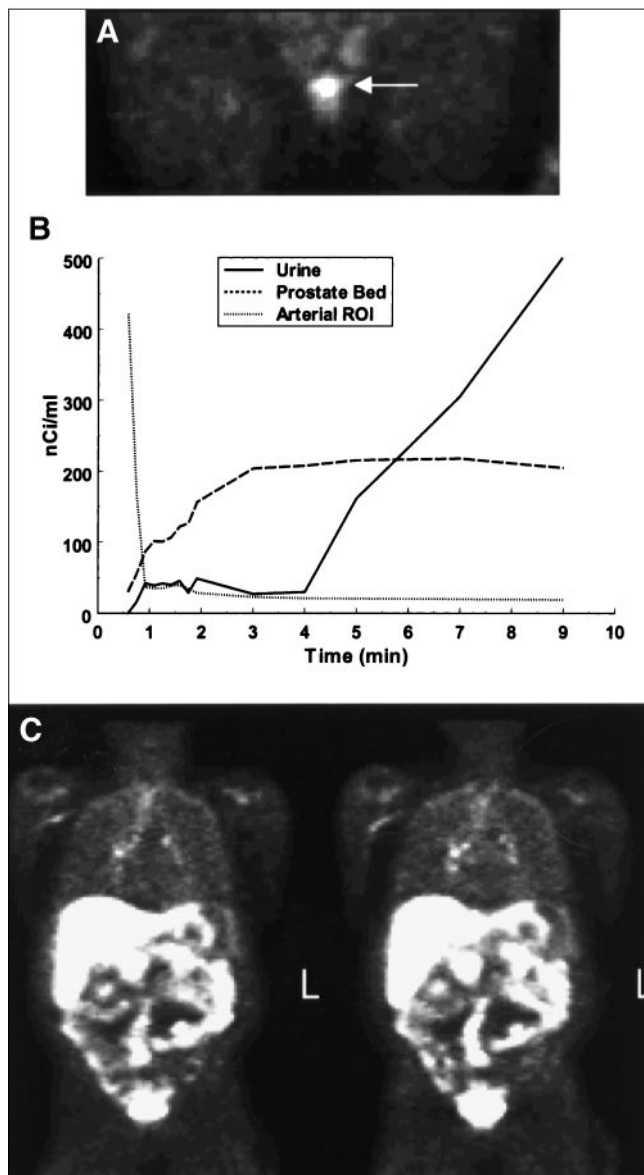


FIGURE 5. (A) Attenuation-corrected FCH PET image (coronal projection, 2–4 min after injection) of pelvic region of patient 1 having biopsy-proven recurrent local prostate carcinoma. Slice thickness is 12.9 mm. In this early image, radioactivity had not yet arrived at urinary bladder, allowing excellent delineation of recurrent disease in prostate bed (arrow). (B) Time-activity curves for FCH in same patient as in A show very rapid clearance of radioactivity from ROI placed on iliac artery, rapid accumulation of tracer in local prostate bed, and arrival of radioactivity in urinary bladder at >4 min after injection. (C) Attenuation-corrected whole-body scan (coronal projections) shows several foci of high FCH uptake in mediastinum suggestive of prostate cancer in hilar and paraaortic lymph nodes. L = left.

tumors: sternal mass (SUV, 14.6), mediastinal and hilar adenopathies (SUVs, ~8.5), and pelvic mass (SUV, 6.5). The parasternal mass appeared significantly larger on the FCH PET scan relative to that on the FDG PET scan. Smaller metastases were indicated on the FCH PET scan in

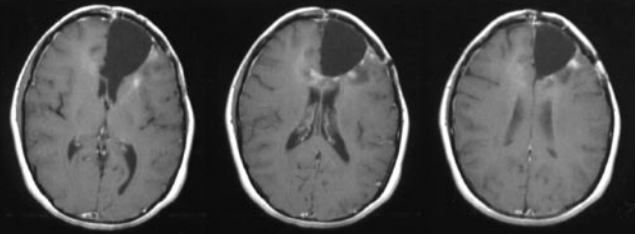
the right chest wall and left lung that were not seen on the FDG PET scan. In reference to the anterior pelvic tumor, a homogeneous distribution of FDG was observed across the tumor in the FDG PET scan, whereas the FCH was preferentially distributed on the periphery of the tumor.

DISCUSSION

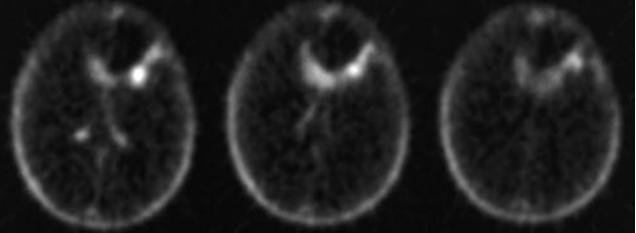
There is a critical need for improved methods to noninvasively detect and monitor treatment of cancer. PET holds unique promise in this regard because of its ability to exploit genetic and biochemical abnormalities present in cancer cells through the use of specific molecular imaging probes. The ideal “magic bullet” for PET of cancer would be a probe that exhibits specific uptake and retention within malignant neoplasms while clearing from the blood and remaining at low concentrations in surrounding normal tissues. Reaching high tumor-to-background ratios in periods consistent with the relatively short half-lives of positron emitters may require the existence of at least 1 normal process by which the tracer is rapidly cleared from the circulation. Other important considerations include the ability to distribute the tracer to PET centers lacking cyclotrons (favoring ^{18}F as radiolabel as opposed to the shorter-lived ^{11}C or use of generator-based isotopes), metabolic handling, dependence on regional perfusion, and sensitivity to systemic factors. For cancer types specific to the pelvic region, such as prostate cancer, the absence of confounding radioactivity in the urinary bladder is also advantageous.

Positron-labeled cholines, as first pioneered by Hara’s research group (4,5,7,9) using ^{11}C as radiolabel and further advanced by our group with introduction of the N - ^{18}F fluoromethyl labeling group (11), appear to have several favorable properties as oncologic PET probes. First, the pathophysiology of choline processing in malignant tissues is well established (20–25). Extensive studies using MR spectroscopy (20) and biochemical analyses (21–25) have revealed elevated levels of choline, phosphocholine, and phosphoethanolamine in many types of cancer cells in consort with enhanced synthesis rates of membrane phospholipids. The activity of CK has been found to be upregulated in malignant cells (22–25), providing a potential mechanism for the enhanced accumulation of radiolabeled choline analogs by neoplasms. These findings have motivated the development of MR spectroscopic imaging techniques for mapping of choline levels in prostate cancer (26,27) and brain tumors (28,29). Second, the rapid and extensive clearance of radiolabeled cholines from the blood after intravenous administration allows commencement of PET of cancer early (2–3 min) after bolus injection of radiotracer. Third, [^{11}C]choline (7) and FCH (11) allow assessment of neoplasms in the pelvis before arrival of radioactivity at the urinary bladder. Finally, the uptake of positron-labeled cholines is very low in normal tissues of the cerebral cortex, lung, heart, bone, and skeletal muscle, allowing excellent differentiation of malignancies against these tissues. Detec-

MRI



[¹⁸F]FCH



[¹⁸F]FDG

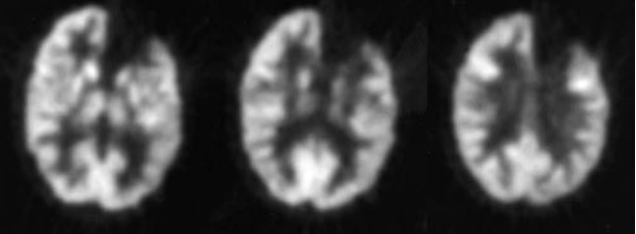
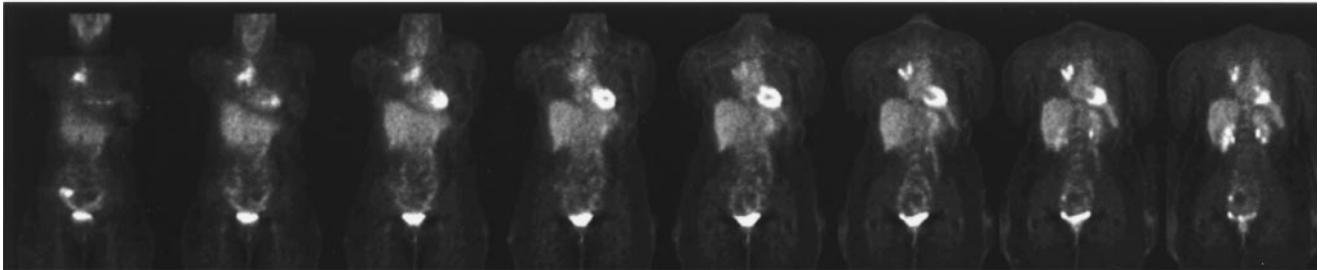


FIGURE 6. Patient with biopsy-confirmed recurrent anaplastic astrocytoma was imaged by T1-weighted Gd-diethylenetriaminepentaacetic acid-enhanced MRI, FCH PET (5–10 min after injection), and FDG PET (30–36 min after injection). MRI shows nodular enhancement posteriorly at postoperative cyst wall. FCH scan shows diffuse abnormal accumulation posteriorly and medially to cyst with focal areas of accumulation corresponding to nodular areas of enhancement on MRI scan. Note absence of normal cortex accumulation that is seen with FCH. FDG scan shows thin rim of abnormal accumulation that would support recurrent tumor, but abnormality is difficult to detect compared with FCH and MRI scans.

FDG-PET



FCH-PET

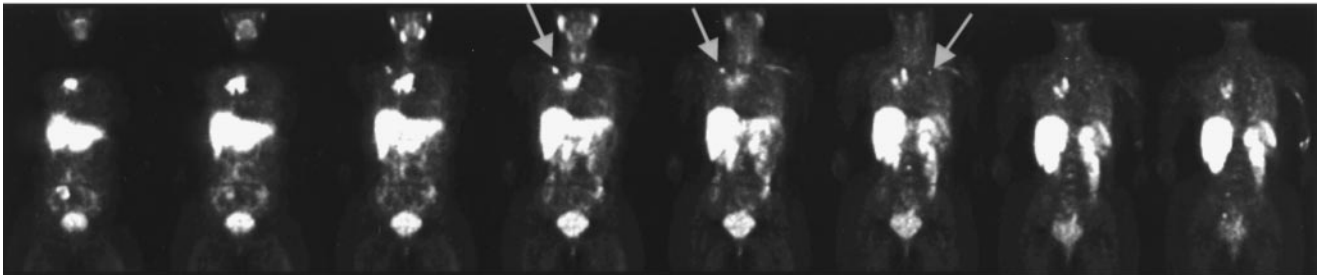


FIGURE 7. Patient with metastatic breast cancer underwent FCH PET and FDG PET. Myocardial uptake is observed only with FDG, whereas more prominent uptake in salivary glands, liver, and kidneys is seen with FCH, which is consistent with normal uptake of choline by these tissues. Uptake of FDG and FCH is indicated in large metastases associated with sternum, right hilar and paratracheal lymph nodes, and right anterior pelvis. Volume of submanubrial metastasis was significantly larger on FCH PET scan. Smaller regions of focal uptake are observed on FCH PET scan in right chest wall and left lung (arrows) that are not seen on FDG PET scan. Uptake pattern of FDG was homogeneous across anterior pelvic metastasis, whereas FCH was taken up preferentially by periphery of this tumor.

tion of malignant adenopathies in the chest is enhanced by low uptake in the lung, heart, and mediastinum (9).

Our results indicate that FCH closely mimics choline in its *in vitro* phosphorylation by yeast CK and uptake and metabolism in cultured human prostate cancer cells. A human CK complementary DNA has been cloned by complementation of the yeast CK mutation, *cki*, from a human glioblastoma complementary DNA expression library (30). The human enzyme was found to resemble the rat liver enzyme over the entire sequence. It also resembled the yeast enzyme in the carboxyl-terminal region, which is thought to be involved in the catalytic function of the enzyme (30). Thus, our results with yeast CK are likely representative of properties of human CK. Further support for the acceptance of FCH by CK is found in the analytic studies of ^{18}F radioactivity after incubation of FCH in cultured PC-3 human prostate cancer cells. After incubation of FCH under control conditions, nearly all ^{18}F radioactivity in the cancer cells is associated with a polar metabolite fraction that exhibits the same HPLC retention time as the single product of *in vitro* incubations of FCH with CK (Fig. 3). The identity of this metabolite was accordingly assigned as P-FCH, although an independent chemical synthesis of P-FCH is desirable for further validation of the analytic results. The apparent IC_{50} values for inhibition of FCH and CH *in vitro* phosphorylation by unlabeled choline of ~ 0.4 mmol/L are high relative to the normal range of choline concentrations in the plasma (0.01–0.1 mmol/L) (31). Pretreatment of cultured PC-3 human prostate cancer cells with 5 mmol/L HC-3, an inhibitor of choline transport and phosphorylation (16,32), resulted in a $>90\%$ decrease in FCH accumulation, evidencing the specificity of FCH for the choline processing pathway. The higher incorporation of FCH relative to ^{14}C choline into lipophilic metabolites in PC-3 cells was a surprising result that requires further investigation.

FCH differs from FEC by a single methylene group between the nitrogen atom and the carbon bearing the fluorine atom. Remarkably, this small structural difference is associated with an 80% decrease in uptake of FEC in PC-3 prostate cancer cells, whereas FMEC, which adds a methylene group to a nonradioactive methyl group, shows only a 50% decrease in tracer accumulation in PC-3 cells. Furthermore, whereas FCH and FMEC showed equivalent *in vitro* phosphorylation with choline, FEC was more poorly phosphorylated by CK (Table 1). Together, these data suggest that an ethyl-for-methyl substitution on choline tracers lowers their affinity for prostate cancer cells but not for CK. Fluorine-for-hydrogen substitution is well tolerated on the methyl group of FCH but is poorly tolerated on the ethyl group of FEC for uptake by PC-3 prostate cancer cells. The progressive decrease in phosphorylation rate as the size of the ^{18}F radiolabel-containing side chain is increased from fluoromethyl to fluoropropyl suggests steric hindrance of CK-catalyzed phosphorylation for analogs having fluorine-containing substituents larger than the fluoromethyl group.

Surprisingly, uptakes of FCH and FPC by PC-3 cells were nearly equivalent despite a large difference in affinity of these 2 tracers for CK-mediated phosphorylation (Table 1). It is possible that the uptakes of FCH and FPC by cultured cancer cells are rate limited at the transport step (33) and the affinity of FCH and FPC for the choline transporter is similar. Accordingly, studies with a broad range of *N*-alkyl substitutions are needed to further clarify the structure–activity relationships for uptake of positron-labeled choline analogs by cancer cells. Although perfusion and transmembrane transport would presumably determine the rate of uptake of the radiolabeled choline analogs by tumors *in vivo*, the phosphorylation process is thought to be essential for metabolic retention of the choline-based tracers within cancer cells.

The preliminary imaging studies show excellent imaging feasibility of FCH in brain tumor, prostate cancer, and breast cancer. Clearly, further clinical studies on a larger number of subjects are needed to evaluate the clinical utility of FCH PET scans in these cancers. The longer half-life of ^{18}F (110 min) is better suited for the demands of clinical PET than is ^{11}C and may allow off-site production and distribution of the radiotracer. The very low uptake of FCH by normal cerebral cortex is a major advantage that FCH appears to share with ^{11}C choline (5) relative to FDG for imaging brain tumors. In prostate cancer, the visualization of cancer in the prostate gland and neighboring tissues early after injection without confounding radioactivity in the urinary bladder is an advantage that FCH appears to share with CH, although later urinary radioactivity may be higher with FCH relative to ^{11}C choline (11). The different pattern of uptake of FDG and FCH in the right anterior pelvic tumor of the breast cancer patient (patient 3) was an interesting finding that may point to differences in the physiology of the 2 tracers. A plausible explanation of the more peripheral deposition of FCH in the tumor relative to FDG is that FCH uptake is more dependent on flow than is FDG uptake and the inner core of this tumor was poorly perfused. FDG has a much slower clearance from the circulation, allowing more time for the tracer to accumulate in poorly perfused tissues. In contrast, the residence time of FCH is very short (<2 min) in the circulation. Perfusion and blood-to-tissue choline transport likely play a major role in the distribution of FCH to tissues, although as noted, phosphorylation and subsequent metabolic steps are presumably involved in retention of the early biodistribution pattern.

CONCLUSION

The findings of upregulation of choline uptake and phosphorylation in neoplasms have motivated the development of positron-labeled choline analogs for PET of cancers. In this work, FCH and CH showed *in vitro* phosphorylation by yeast CK and HC-3-sensitive accumulation and phosphorylation in cultured PC-3 human prostate cancer cells. Fluoroethyl (FEC) and fluoropropyl (FPC) choline analogs

showed relatively poorer acceptance by CK. Radiation dosimetry estimates for FCH show the kidney to be the dose-critical organ. Preliminary PET studies on patients with prostate and breast cancer and on a patient with a brain tumor revealed uptake of FCH in neoplasms. These data indicate that the fluoromethylated tracer, FCH, closely mimics choline uptake and sequestration in cancer cells and support the need for future investigations to determine the sensitivity and accuracy of FCH PET for detection, staging, and evaluation of cancer.

ACKNOWLEDGMENTS

The authors thank technologists Mary Traynor and De-Andre Starnes for their excellent assistance and appreciate the clinical collaborations with Drs. P. Kelly Marcom, Matthew J. Ellis, Michael J. Kelley, and Allan H. Friedman.

REFERENCES

- Weber WA, Avril N, Schwaiger M. Relevance of positron emission tomography (PET) in oncology. *Strahlenther Onkol.* 1999;175:356–373.
- Delbeke D. Oncological applications of FDG PET imaging: brain tumors, colorectal cancer, lymphoma, and melanoma. *J Nucl Med.* 1999;40:591–603.
- Hoh CK, Seltzer MA, Franklin J, deKernion JB, Phelps ME, Bellegrun A. Positron emission tomography in urological oncology. *J Urol.* 1998;159:347–356.
- Hara T, Kosaka N, Shinoura N, Kondo T. PET imaging of brain tumor with [methyl-¹¹C]choline. *J Nucl Med.* 1997;38:842–847.
- Shinoura N, Nishijima M, Hara T, et al. Brain tumors: detection with C-11 choline PET. *Radiology.* 1997;202:497–503.
- Marriott CJ, Thorstad W, Akabani G, et al. Locally increased uptake of fluorine-18-fluorodeoxyglucose after intracavitary administration of iodine-131-labeled antibody for primary brain tumors. *J Nucl Med.* 1998;39:1376–1380.
- Hara T, Kosaka N, Kishi H. PET imaging of prostate cancer using carbon-11-choline. *J Nucl Med.* 1998;39:990–995.
- Shreve PD, Grossman HB, Gross MD, Wahl RL. Metastatic prostate cancer: initial findings of PET with 2-deoxy-2-[¹⁸F]-fluoro-D-glucose. *Radiology.* 1996;199:751–756.
- Kobori O, Kirihara Y, Kosaka N, Hara T. Positron emission tomography of esophageal carcinoma using ¹¹C-choline and ¹⁸F-fluorodeoxyglucose: a novel method of preoperative lymph node staging. *Cancer.* 1999;86:1639–1648.
- Hara T, Yuasa M, Yoshida H. Automated synthesis of fluorine-18 labeled choline analogue: 2-fluoroethyl-dimethyl-2-oxyethylammonium [abstract]. *J Nucl Med.* 1997;38(suppl):44P.
- DeGrado TR, Coleman RE, Wang S, et al. Synthesis and evaluation of ¹⁸F-labeled choline as an oncologic tracer for positron emission tomography: initial findings in prostate cancer. *Cancer Res.* 2001;61:110–117.
- Block D, Coenen HH, Stöcklin G. The N.C.A. nucleophilic ¹⁸F-fluorination of 1,N-disubstituted alkanes as fluoroalkylation agents. *J Labelled Compd Radiopharm.* 1987;24:1029–1042.
- Roivainen A, Forsback S, Groenroos T, et al. Blood metabolism of [methyl-¹¹C]choline: implications for in vivo imaging with positron emission tomography. *Eur J Nucl Med.* 2000;27:25–32.
- Pomfret EA, daCosta K-A, Schurman LL, Zeisel SH. Measurement of choline and choline metabolite concentrations using high-pressure liquid chromatography and gas chromatography-mass spectrometry. *Anal Biochem.* 1989;180:85–90.
- Ishidate K, Nakazawa Y. Choline/ethanolamine kinase from rat kidney. *Methods Enzymol.* 1992;209:121–123.
- Hernández-Alcoceba R, Saniger L, Campos J, et al. Choline kinase inhibitors as a novel approach for antiproliferative drug design. *Oncogene.* 1997;15:2289–2301.
- Kirschner AS, Ice RD, Beierwaltes WH. Radiation dosimetry of ¹³¹I-19-iodocholesterol: the pitfalls of using tissue concentration data [reply to letter]. *J Nucl Med.* 1975;16:248–249.
- Stabin M. MIRDose: the personal computer software for use in internal dose assessment in nuclear medicine. *J Nucl Med.* 1996;37:538–546.
- DeGrado TR, Turkington TG, Williams JJ, Stearns CW, Hoffman JM, Coleman RE. Performance characteristics of a whole-body PET scanner. *J Nucl Med.* 1994;35:1398–1406.
- Negendank W. Studies of human tumors by MRS: a review. *NMR Biomed.* 1992;5:303–324.
- Kano-Sueoka T, Watanabe T, Miya T, Kasai H. Analysis of cytosolic phosphoethanolamine and ethanolamine and their correlation with prognostic factors in breast cancer. *Jpn J Cancer Res.* 1991;82:829–834.
- Macara IG. Elevated phosphocholine concentration in ras-transformed NIH3T3 cells arises from increased choline kinase activity, not from phosphatidylcholine breakdown. *Mol Cell Biol.* 1989;9:325–328.
- Ratnam S, Kent C. Early increase in choline kinase activity induction of the H-ras oncogene in mouse fibroblast cell lines. *Arch Biochem Biophys.* 1995;323:313–322.
- Nakagami K, Uchida T, Ohwada S, et al. Increased choline kinase activity and elevated phosphocholine levels in human colon cancer. *Jpn J Cancer Res.* 1999;90:419–424.
- Bhakoo KK, Williams SR, Florian CL, Land H, Noble MD. Immortalization and transformation are associated with specific alterations in choline metabolism. *Cancer Res.* 1996;56:4630–4635.
- Scheider J, Hricak H, Vigneron DB, et al. Prostate cancer: localization with three-dimensional proton MR spectroscopic imaging—clinicopathologic study. *Radiology.* 1999;213:473–480.
- Yu KK, Scheider J, Hricak H, et al. Prostate cancer: prediction of extracapsular extension with endorectal MR imaging and three-dimensional proton MR spectroscopic imaging. *Radiology.* 1999;213:481–488.
- Heesters MAAM, Go KG, Kamman KL, et al. ¹¹C-tyrosine positron emission tomography and ¹H magnetic resonance spectroscopy of the response of brain gliomas to radiotherapy. *Neuroradiology.* 1998;40:103–108.
- Preul MC, Leblanc R, Caramanos Z, Kasrai R, Narayanan S, Arnold DL. Magnetic resonance spectroscopy guided brain tumor resection: differentiation between recurrent glioma and radiation change in two diagnostically difficult cases. *Can J Neurol Sci.* 1998;25:13–22.
- Hosaka K, Tanaka S, Nikawa J, Yamashita S. Cloning of a human choline kinase cDNA by complementation of the yeast *cki* mutation. *FEBS Lett.* 1992;304:229–232.
- Bligh J. The level of free choline in plasma. *J Physiol.* 1952;117:234–240.
- Guyenet P, Lefresne P, Rossier J, Beaujouan JC, Glowinski J. Inhibition by hemicholinium-3 of (¹⁴C)acetylcholine synthesis and (³H)choline high-affinity uptake in rat striatal synaptosomes. *Mol Pharmacol.* 1973;9:630–639.
- Katz-Brull R, Degani H. Kinetics of choline transport and phosphorylation in human breast cancer cells: NMR application of the zero trans method. *Anticancer Res.* 1996;16:1375–1380.